RSC Advances

ROYAL SOCIETY OF CHEMISTRY

www.rsc.org/advances

RSC Advances

Characterization of porous bismuth oxide (Bi$_2$O$_3$) nanoplates prepared by chemical bath deposition and post annealing

Ying Wang, [a] Liangxing Jiang, *[a] Ding Tang, [a] Fangyang Liu, [a] and Yanqing Lai [a]

Porous β-Bi$_2$O$_3$ nanoplates were firstly synthesized on FTO substrate via chemical bath deposition followed by annealing. It showed higher photoinduced current density than nonporous ones though the former possessed larger band gap. The as prepared photoelectrodes exhibited superior stability in aqueous solutions. The results illustrates that the porous Bi$_2$O$_3$ nanoplate films have potential in the application of photoelectrocatalysis.

1. Introduction

Bismuth oxide (Bi$_2$O$_3$) has been widely used in supercapacitors, optoelectronic devices, gas sensors, solar cells etc., owing to its high specific capacitance, high electrochemical stability and marked photoluminescence properties[1-4]. In addition, bismuth oxide is an excellent candidate for photocatalysis because of its specific properties. For instance, bismuth oxide is an intrinsic n-type semiconductor with four crystalline phases possessing different band gaps, which means a better band engineering according to different cases of photocatalysis[5]. Moreover, the valence band of bismuth oxide is made of hybrid Bi 6s and O 2p orbit that decreases the symmetry of the band structure and leads to the corresponding dipoles which could enhance the photocatalytic activity[6]. At last, bismuth oxide is an environmental friendly material.

So far, various synthetic methods were explored to prepare nanostructured Bi$_2$O$_3$. For example, Bi$_2$O$_3$ nanospheres, nanosheets, nanorods and nanorings were successfully synthesized via solvothermal methods or hydrothermal processes[7-9]. Cube-like β-Bi$_2$O$_3$ microcrystals and monoclinic α-Bi$_2$O$_3$ were also fabricated by precipitation and calcination of hydrothermally prepared (BiO)$_2$CO$_3$ precursor, respectively[10, 11]. All the above products exhibited outstanding visible-light-driven photocatalytic performance in pollution elimination. Nevertheless, the high cost of energy, time and raw materials required in above mentioned processes should be considered. Moreover, the recycling of Bi$_2$O$_3$ nanocrystals would be a big problem. In order to circumvent the above problems and improve the efficiency of photocatalysis by taking advantage of bias

voltage, Bi$_2$O$_3$ thin films were also prepared for both photocatalysis and photoelectrocatalysis. Anodization of bismuth foil[12-14], dip-coating[15] and chemical vapour deposition[16, 17] were employed for preparing Bi$_2$O$_3$ thin films. However, the samples fabricated by above methods showed a relatively large band gap ($\geq$2.48eV) and the 1-dimensional nanoporous morphology, which would limit the efficiency of photoelectric conversion and photoelectrocatalytic activity. Additionally, other approaches such as electrospun can't satisfy the requirement of low cost and high photoelectrocatalysis performance[18, 19]. Thus, Mane et al. [3-5] proposed a mild solution route called the chemical bath deposition (CBD) to fabricate the Bi$_2$O$_3$ nanoplate thin films. In this simple aqueous system, the NO$_3^-$ ions benefited the crystal growth along the [001] direction to obtain needle-like Bi$_2$O$_3$ crystals. While, OH$^-$ tended to be absorbed on the (001) face and suppressed the preferred growth in the [001] direction owing to the shielding effect[9, 20]. Therefore, it is convenient to achieve the morphology controlling by just changing the ratio of raw materials. The Bi$_2$O$_3$ nanoplate thin films synthesized by Mane et al. [3-5] were used as carbon dioxide gas sensor and photoanodes in dye-sensitized solar cells. However, the controlling of the experimental conditions exactly to achieve the morphology evolution has not been reported.

On the base of the above reasons, the hierarchical self-assemble porous β-Bi$_2$O$_3$ nanoplate thin films which were different from Mane et al. [3-5] were fabricated on FTO (Fluorine-doped tin oxide) through CBD process and post annealing, and characterized as photoelectrode material in photoelectrocatalysis for the first time. The nonporous β-Bi$_2$O$_3$ nanoplate thin films were also produced for comparison. And the different growth mechanisms of porous and nonporous β-Bi$_2$O$_3$ nanoplates were revealed firstly.

2. Experimental

2.1. Synthesis

The Bi$_2$O$_3$ thin films were synthesized in an aqueous media in open system. All reagents used in the experiment were of analytical grade and used without further purification. FTO glass substrates were ultrasonically cleaned sequentially in detergent-added

a School of Metallurgy and Environment, Central South University, Changsha 410083,China. E-mail: lxjiang@csu.edu.cn, Tel: +86 731 88830474; Fax: +86 731 88876454.

distilled water, acetone and isopropyl alcohol. The porous Bi_2O_3 nanoplate thin films (marked as sample A) were synthesized via the following processes. Firstly, 3 mL triethanolamine was added into 60 mL $Bi(NO_3)_3$ solution (0.1 M). After stirring for 15 minutes, KOH was added to adjust the pH to 13.5. After that, the clean FTO glass slides were vertically immersed in the above solution and maintained at 60 ℃ for 2 h. The as-deposited films were annealed in air at 350 ℃ for 60 min with heating rate of 5 ℃/min, and then cooled down to room temperature naturally. The nonporous Bi_2O_3 nanoplate thin films (marked as sample B) were fabricated through the similar and typical method described in the previous literature[4].

2.2. Characterization

The crystalline properties and morphology of the prepared films were characterized by X-ray diffractometer (XRD, Rigaku3014) equipped with Cu Kα radiation (λ=1.54 Å), environmental scanning electron microscope (ESEM, FEI Quanta-200 at a 20 keV accelerating voltage) and transmission electron microscopy (TEM, JEOL JEM-2100F; accelerating voltage: 200 kV). High-resolution transmission electron microscopy (HRTEM) images were obtained by using JEM 2100F field-emission transmission electron microscope operated at an accelerating voltage of 200 kV. The composition of the prepared films was determined by X-Ray Fluorescence (Shimadzu XRF-1800) operated under 35℃ with high vacuum at a working voltage and current of 40 kV and 95 mA, respectively. The transmittance spectra of the samples were conducted using an UV-Vis-NIR spectrophotometer (HITACHI U-4100) in a wavelength range of 300-900 nm at room temperature. There was a relationship between the band gap and the optical absorption defined as Tauc relation: $\alpha h\nu = A(h\nu - Eg)^n$. Here, α is the absorption coefficient, A is a constant, ($h\nu$) is the photon energy, the n is 2 for Bi_2O_3 with indirect transitions[21]. The photoelectrochemical (PEC) characterization of the film was carried out in 1 M NaOH solution in a Pyrex electrolytic cell, where the sample, a high-purity graphite plate, and a SCE were used as the working, counter and reference electrode, respectively. A 300 W xenon lamp was used as the light source with the light intensity kept at 40 mW/cm^2.

3. RESULTS AND DISCUSSION

3.1. Composition and Structure

The composition of sample A and B was shown in table 1. The ratios of Bi and O were 1: 1.8 and 1: 1.75 for sample A and B, respectively, which were close to the ideal composition of Bi_2O_3 (Bi: O=1: 1.5).

Table 1: The composition of sample A and B

Sample	Atomic percentage (%)	
	Bi	O
A	35.30	64.70
B	36.24	63.76

The crystal structure of the prepared film (sample A and B) was characterized by XRD (Figure 1). All the diffraction peaks can be

indexed to tetragonal phase β-Bi_2O_3 (JCPDS card No.78–1793) with preferred orientation in (201) direction. No other crystalline impurities were detected, demonstrating the phase purity of the Bi_2O_3 products. Moreover, the Full Width at Half Maximum (FWHM) of main peak (201) for sample A (0.216 °) is smaller than that of sample B (0.274 °). The results illustrated that sample A occupied a higher degree of crystallinity[22].
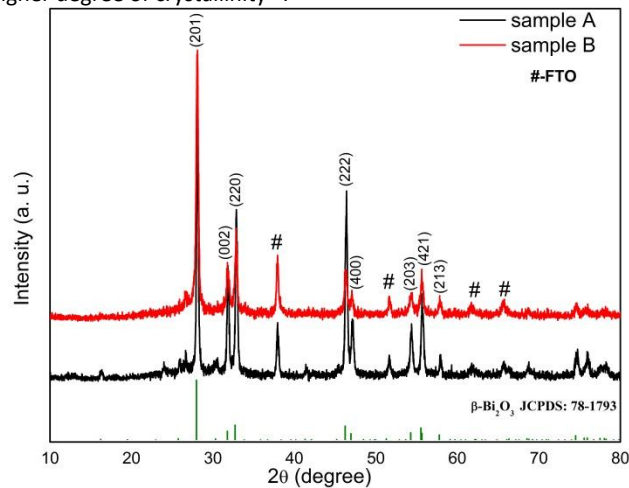

Figure 1: XRD spectra of sample A and B

Because the Bi_2O_3 nanoplates were fabricated on the FTO substrate, the yellow thin film was scraped off and dispersed in alcohol sufficiently via vigorous ultrasonic treatment for TEM characterization. Though some nanosheets overlapped, the nanocrystals were almost homogenous as shown in Figure 2a. The average diameter of nanoplates is 20~35 nm from the corresponding size distribution chart given in Figure 2b. The high-resolution TEM images (Figure 2c) revealed that the nanoplates were of multi-crystal structure. The lattice fringe taken with the electron beam perpendicular to the surface of a nanosheet was clear. The interplanar spacings were 0.326 nm and 0.346 nm, which corresponded to the (201) and (210) planes of tetragonal Bi_2O_3, respectively. The lattice data calculated from a selected area electron diffraction (SAED) pattern (Figure 2d) of a randomly chosen region of the nanosheets can be indexed to the lattice parameters of β-Bi_2O_3. Both the HRTEM and SAED analyses indicated [201] was the preferential growth direction and the synthesized products possessed the structure of tetragonal β-Bi_2O_3.
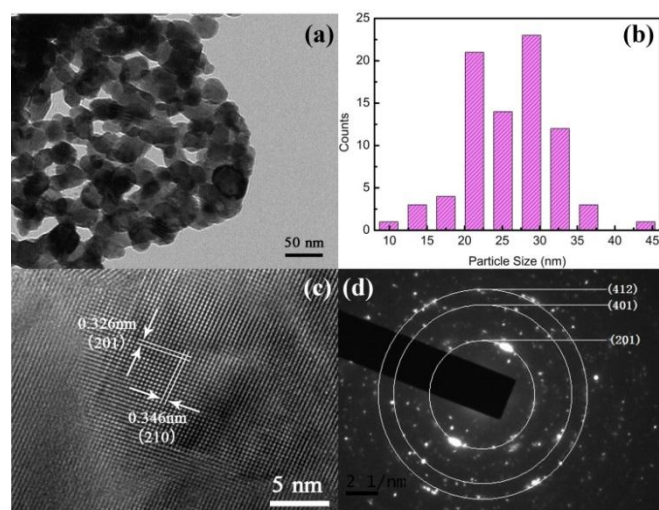
Journal Name COMMUNICATION

Figure 2: (a) Low-magnification TEM image of the Bi_2O_3 nanoplates; (b) distribution plot of the as-synthesized nanoplates; (c) HRTEM images of the nanoplates; (d) The corresponding SAED pattern of the nanoplates.

3.2. Morphology

The morphology of the sample A and B was characterized by SEM. The typical magnification SEM image (Figure 3a) of sample A clearly revealed that the sample film consisted of uniform nanoplates which were perpendicular with certain angle to the substrate surface and intercrossed with each other. Additionally, all the nanoplates of sample A presented an obvious porous structure with the ragged edge, which was beneficial to photoelectrocatalytic applications and would illustrate in the next section. As for the sample B, there were some big particles on the film when observed by naked eyes, which were not as smooth as the sample A. The SEM images of sample B were shown in Figure 3c. Thinker nanoplates with relatively dense and smooth surface were observed. Figure 3b and 3d showed the corresponding cross-sectional SEM images, demonstrating the thickness of the film was 3.28 μm and 3.59 μm for sample A and B, respectively.

Figure 3 also revealed the different crystal growth mechanism of sample A and B. Figure 3a and 3b demonstrated that the perforation plate morphology of the Bi_2O_3 films is formed by the aggregation of nanoparticles[21]. While major growth mechanism of the thick Bi_2O_3 nanoplates with smooth surface in figure 3c and 3d was Ostwald ripening, this was similar to that of CuO nanoplates reported by Li et al[23].
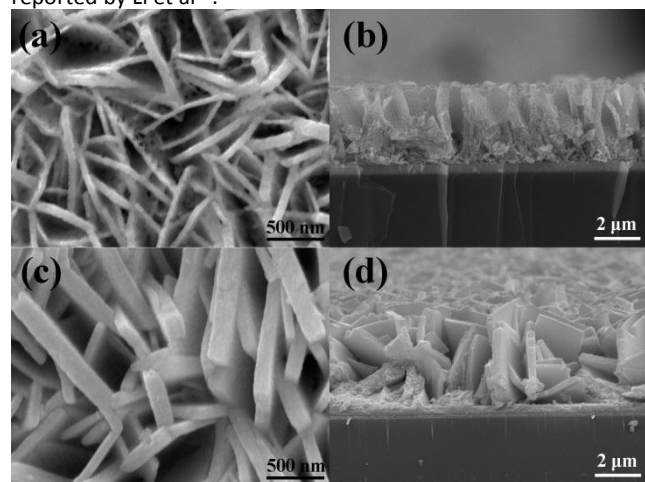

3.3. Optical and photoelectrochemical properties

UV-vis spectroscopy was utilized for measuring the optical properties of sample A and B, and the results were shown in Figure 4. The sharp absorption edge in Figure 4a inferred that the band gap was due to the intrinsic transition of the Bi_2O_3 nanoplates but not the impurity[24]. The band gap values, obtained by extrapolating the straight portion of the curve achieved via $(\alpha h v)^2$ against hv plots to the point where $\alpha=0$, were 2.22 and 2.18 eV for sample A and B, respectively. They were both a little smaller than the reported value (2.47 eV)[25]. The same phenomenon was also observed by Xie et al.[26] who had reported that the Bi_2O_3 nanosheets displayed narrower band gap than the nanosheet-covered ones and porous Bi_2O_3 microrods due to the different morphology and size. As the band gap of sample B was smaller than that of sample A, it seemed that the sample B may had larger absorption range and higher photo energy utilization efficiency of the sunlight and thus more efficient on photocatalysis.

Figure 3: Plane-views of sample A (a) and B(c). Corresponding Cross-sectional SEM images of sample A (b) and B (d).
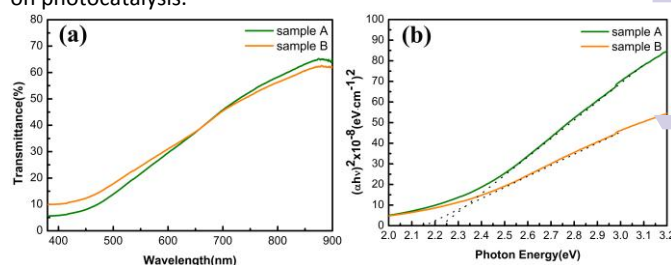

Figure 4: (a) Transmittance spectra of sample A and sample B; (b) Corresponding optical band gap calculations.

In order to evaluate the photoelectrochemical performance of the Bi_2O_3 nanoplate films for water oxidation, photocurrent-potential response experiments were carried out under chopped light. The results were displayed in Figure 5. All the samples showed a perfect response in the positive potential, which deduced the Bi_2O_3 films were n-type semiconductors. Sample A showed the better photo-response (~10 μA/cm² at 0.90 V vs SCE) than the sample B (~2 μA/cm², at 1.0 V vs SCE) though the latter possessed a smaller band gap, which meant the sample A owned the better photoelectrical conversion efficiency. It can be illustrated by the hierarchical porous structure of Bi_2O_3 film as observed by SEM. On one hand, sample A has a higher degree of crystallinity and lower Bi/O ratio comparing to sample B, which is beneficial to the photoreponse[27]. On the other hand, the porous structure of the nanoplates would lead to the larger specific surface area which contributed to more favorable adsorption of OH^- over the surface of photocatalysts and enhance the photocatalytic activity[28]. Moreover, the porous nanoplates with certain angle perpendicular to the substrate surface would lengthen the incident path of light due to multiplex refraction and make for ideally random light-trapping[13, 29, 30].

A photo-current versus time evolution of the photoelectrolysis system for photoelectrochemical oxidation of water was shown in Figure 5b. After 460 seconds of photoelectrochemical experiment, the photocurrent stabilized at its original level, indicating that the

photocatalyst would have the potential to validly prevent photocorrosion under long irradiation.
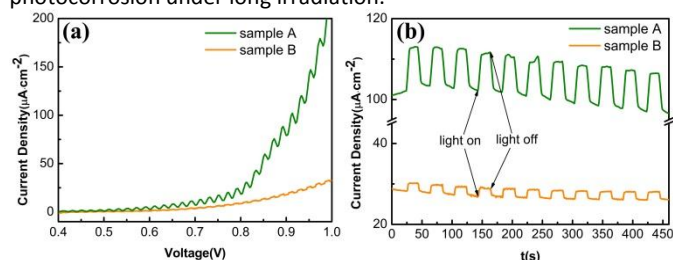

Figure 5: (a) *J-V* scans of sample A and B; (b) Transient photocurrent response curves of sample A and B. A 300 W xenon lamp was used as the light source with the light intensity kept at 40 mW/cm², and the scan rate is 2 mV/s.

Conclusions

The hierarchical porous β-Bi$_2$O$_3$ nanoplate thin films on transparent FTO substrates have been successfully synthesized through a facile chemical bath deposition followed by annealing process for the first time. Due to the larger specific surface area and better light-trapping as the porous nanoplates were perpendicular to the substrate surface at a certain angle, the photocurrent density obtained from porous β-Bi$_2$O$_3$ nanoplate films was 5 fold higher than that of typical nonporous nanoplate films, even though the former has the larger band gap. The results revealed that the hierarchical porous β-Bi$_2$O$_3$ nanoplate thin film would be a promising candidate for photoelectrocatalysis of water splitting.

Acknowledgements

References

1.   F. L. Zheng, G. R. Li, Y. N. Ou, Z. L. Wang, C. Y. Su and Y. X. Tong, *Chem Commun (Camb)*, 2010, **46**, 5021-5023.

2.   H. T. Fan, X. M. Teng, S. S. Pan, C. Ye, G. H. Li and L. D. Zhang, *Appl Phys Lett*, 2005, **87**, 231916.

3.   S. S. Bhande, R. S. Mane, A. V. Ghule and S.H. Han, *Scripta Materialia*, 2011, **65**, 1081-1084.

4.   S. M. F. Shaikh, G. Rahman, R. S. Mane and O.S. Joo, *Electrochim Acta*, 2013, **111**, 593-600.

5.   T. P. Gujar, V. R. Shinde, C. D. Lokhande, R. S. Mane and S.H. Han, *Appl Surf Sci*, 2005, **250**, 161-167.

6.   H. Cheng, B. Huang, J. Lu, Z. Wang, B. Xu, X. Qin, X. Zhang and Y. Dai, *Phys Chem Chem Phys*, 2010, **12**, 15468-15475.

7.   F. Qin, H. Zhao, G. Li, H. Yang, J. Li, R. Wang, Y. Liu, J. Hu, H. Sun and R. Chen, *Nanoscale*, 2014, **6**, 5402-5409.

8.   M. Faisal, A. A. Ibrahim, H. Bouzid, S. A. Al-Sayari, M. S. Al-Assiri and A. A. Ismail, *Journal of Molecular Catalysis A: Chemical*, 2014, **387**, 69-75.

9.   H. Lu, S. Wang, L. Zhao, B. Dong, Z. Xu and J. Li, *Rsc Adv*, 2012, **2**, 3374.

10.   Z. Ai, Y. Huang, S. Lee and L. Zhang, *J Alloy Compd*, 2011, **509**, 2044-2049.

11.   Y. Lu, Y. Zhao, J. Zhao, Y. Song, Z. Huang, F. Gao, N. Li and Y. Li, *Cryst Growth Des*, 2015, **15**, 1031-1042.

12.   X. Lv, J. Zhao, X. Wang, X. Xu, L. Bai and B. Wang, *J Solid State Electr*, 2013, **17**, 1215-1219.

13.   X. Yang, X. Lian, S. Liu, G. Wang, C. Jiang, J. Tian, J. Chen and R. Wang, *Journal of Physics D: Applied Physics*, 2013, **46**, 035103.

14.   K. C. Chitrada, K. S. Raja, R. Gakhar and D. Chidambaram, *J Electrochem Soc*, 2015, **162**, H380-H391.

15.   J. L. Ropero-Vega, A. M. Meléndez, J. A. Pedraza-Avella, R. J. Candal and M. E. Niño-Gómez, *J Solid State Electr*, 2014, **18**, 1963-1971.

16.   D. Barreca, G. A. Rizzi and E. Tondello, *Thin Solid Films*, 1998, **333**, 35-40.

17.   G. Bandoli, D. Barreca, E. Brescacin, G. A. Rizzi and E. Tondello, *Chemical Vapor Deposition*, 1996, **2**, 238-242.

18.   T. N. Soitah, Y. Chunhui, Y. Yong, N. Yinghua and S. Liang, *Current Applied Physics*, 2010, **10**, 1372-1377.

19.   K. Brezesinski, R. Ostermann, P. Hartmann, J. Perlich and T. Brezesinski, *Chem Mater*, 2010, **22**, 3079-3085.

20.   Y.C. Wu, Y.C. Chaing, C.Y. Huang, S.F. Wang and H.Y. Yang, *Dyes and Pigments*, 2013, **98**, 25-30.

21.   C. Zhu and M. J. Panzer, *Chem Mater*, 2014, **26**, 2960-2966.

22.   H. Lim, E. Yilmaz and H. R. Byon, *The Journal of Physical Chemistry Letters*, 2012, **3**, 3210-3215.

23.   Y. Li, B. Tan and Y. Wu, *Chem Mater*, 2008, **20**, 567-576.

24.   C. Zhang and Y. Zhu, *Chem Mater*, 2005, **17**, 3537-3545.

25.   G. Cai, L. Xu, B. Wei, J. Che, H. Gao and W. Sun, *Materials Letters*, 2014, **120**, 1-4.

26.   D. Xie, Q. Su, J. Zhang, G. Du and B. Xu, *J Mater Sci*, 2013, **49**, 218-224.

27.   M. E. Rincón, M. Sánchez, P. J. George, A. Sánchez and P. K. Nair, *Journal of Solid State Chemistry*, 1998, **136**, 167-174.

28.   X. Yang, X. Lian, S. Liu, C. Jiang, J. Tian, G. Wang, J. Chen and R. Wang, *Appl Surf Sci*, 2013, **282**, 538-543.

29.   M. D. Kelzenberg, S. W. Boettcher, J. A. Petykiewicz, D. B. Turner-Evans, M. C. Putnam, E. L. Warren, J. M. Spurgeon, R. M. Briggs, N. S. Lewis and H. A. Atwater, *Nat Mater*, 2010, **9**, 239-244.

30.   L. Chen, J. He, Q. Yuan, Y. Liu, C.T. Au and S.F. Yin, *J Mater Chem A*, 2015, **3**, 1096-1102.